In vitro degradation and cytocompatibility of a low temperature in-situ grown self-healing Mg-Al LDH coating on MAO-coated magnesium alloy AZ31

Chang-Yang Li[a,1], Ling Gao[b,c,1], Xiao-Li Fan[a], Rong-Chang Zeng[a,d,*], Dong-Chu Chen[e], Ke-Qian Zhi[b,c,**]

[a] Corrosion Laboratory for Light Metals, College of Materials Science and Engineering, Shandong University of Science and Technology, Qingdao, 266590, China
[b] Department of Oral and Maxillofacial Surgery, The Affiliated Hospital of Qingdao University, Qingdao, Shandong, 266555, China
[c] Key Lab of Oral Clinical Medicine, The Affiliated Hospital of Qingdao University, Qingdao, Shandong, 266555, China
[d] School of Materials Science and Engineering, Zhengzhou University, Zhengzhou, 450002, China
[e] School of Materials Science and Energy Engineering, Foshan University, Foshan, 528000, China

A B S T R A C T

Basically, Mg–Al layered double hydroxide (LDH) coatings are prepared on the surface of micro-arc oxidation (MAO) coated magnesium (Mg) alloys at a high temperature or a low pH value. This scenario leads to the growth rate of LDH coating inferior to the dissolution rate of the MAO coating. This in turn results in limited corrosion resistance of the composite coating. In this study, a Mg–Al LDH coating on MAO-coated Mg alloy AZ31 is prepared through a water bath with a higher pH (13.76) at a lower temperature (60 °C). FE-SEM, EDS, XRD, XPS, and FT-IR are applied to analyze the surface morphology, chemical compositions, and growth process. Electrochemical polarization, electrochemical impedance spectroscopy (EIS) and hydrogen evolution tests are employed to evaluate the corrosion resistance of the samples. The results disclose that the MAO coating is completely covered by the nanosheet-structured LDH coating with a thickness of approximately 3.8 μm. The corrosion current density of the MAO-LDH composite coating is decreased four orders of magnitude in comparison to its substrate; the presence of a wide passivation region in anodic polarization branch demonstrates its strong self-healing ability, indicating the hybrid coating possesses excellent corrosion resistance. The formation mechanism of the LDH coating on the MAO-coated Mg alloy is proposed. Furthermore, the cytocompatibility is assessed via an indirect extraction test for MC3T3-E1 pre-osteoblasts, which indicates an acceptable cytocompatibility of osteoblasts for the composite coating.

1. Introduction

Magnesium (Mg) alloys, with good biocompatibility, degradability and the elastic modulus similar to human bone, have become the preferred materials for bone implant materials [1–3]. The degradability of Mg alloys not only avoid the secondary surgery, but also reduce the patient's pain and cost [4]. However, chemically active Mg alloys are highly susceptible to biodegradation in in vivo environment and thus lose their mechanical strength prematurely, which results in its difficulty to serve a complete life as bone implants [5,6]. Therefore, it is an important issue to regulate the degradation of Mg alloys at a reasonable

rate. Currently, micro-arc oxidation (MAO), as one of the surface modification techniques [7–9], which has a high-strength and adhesion to its substrate, is a good choice for the purpose. However, porous structure of the MAO coating is considered a serious threat to as-expected high corrosion resistance [10]. The reason is that the aggressive medium can easily penetrate the interface of the MAO/substrate through the through pores, resulting in the galvanic corrosion between the MAO coating and substrate [11]. Hence, it is necessary to build a top layer to seal the porous MAO coating.

Layered double hydroxide (LDH) is a nanostructured material, and has a sandwich-like structure with bivalent and trivalent cations

encapsulating anions [12–14]. On the one hand, it can act as a physical barrier to inhibit corrosion. On the other hand, it also has an ion-exchangeable ability [15,16], which can effectively reduce the damage caused by Cl^- ions in corrosive media. This is because Cl^- ions in the solution diffuse onto the solution/coating interface, and are absorbed and detained by intercalation anion CO_3^{2-} of the LDH. The result avoids the formation of soluble chlorides in the coating. At the same time, CO_3^{2-} ions released from the LDH intercalation layer diffuse into the coating/solution interface and concentrate on the coating surface to form a diffusion boundary layer. As a result, the concentration of CO_3^{2-} ions overwhelms that of Cl^- ions at the coating/solution interface. The content of Cl^- ions is reduced through competitive adsorption [17]. Notably, LDH coating, with a nano-network structure, increases the adhesion, migration and proliferation of cells, resulting in improvement on biocompatibility [18–20]. Overall, to construct LDH coating as the top layer of the MAO coating is an effective and feasible approach.

Currently, the preparation of the LDH coating includes physical deposition and *in situ* growth methods. Physical deposition is to deposit the LDH powders on the substrate through spin or spray ways; but the coating has a poor bonding strength with the substrate. While *in situ* growth method includes hydrothermal treatment (*e.g.* urea), co-precipitation and steam and water bath as well [21–25]. For example, Ishizaki et al. [22] prepared a Mg–Al LDH coating with a high-pressure steam method via setting Mg alloy AZ31 into a 100 mL Teflon-lined autoclave containing 20 mL of ultra-pure water at 160 °C for 6 h. The result indicates the Mg–Al LDH coating has a dense structure and good corrosion resistance. Chen et al. [24–26] fabricated a Mg–Al LDH coating using water bath at a low temperature. Firstly, a carbonic acid solution was prepared through bubbling CO_2 gas. And 0.5 mol L^{-1} Na_2CO_3 was added into the carbonic acid solution, and then pure aluminum (Al) plate was dissolved to Al^{3+}-saturated solution, adjusting the pH to 10.5 with 2 mol L^{-1} NaOH solution. Mg substrates were subsequently immersed in the pretreated-carbonic acid solution, and the CO_2 gas was continuously bubbled at 60 °C for 30 min. Finally, the pretreated Mg alloys were immersed in the above Al^{3+}-saturated solution at 80 °C for 1.5 h. This also obtained a LDH coating with good corrosion resistance. However, the preparation parameters at a high temperature or/and a low pH value may be not suitable for the preparation of Mg–Al LDH on MAO coatings.

This issue involves the mismatch between the dissolution rate of the MAO coating and the growth rate of the LDH coating during LDH preparation process. Firstly, if the dissolution rate of the MAO coating is greater than the growth rate of the LDH coating, the corrosion resistance of the composite coating may be limited. For example, Chen et al. [27] prepared a Mg–Al-LDH on MAO-coated Mg alloy AZ31 through hydrothermal treatment in 0.1 M $Al(NO_3)_3$ and 0.6 M NH_4NO_3 solution at 95 °C with a pH of 7 for 1 h. The results reveal a low pH value results in cracking in the MAO coating. And the corrosion current density (i_{corr}) of the composite coating instead increased one order of magnitude than that of the MAO coating, which demonstrates that the corrosion resistance of the hybrid coating cannot reach the as-expected target.

Secondly, if the dissolution rate of the MAO coating is equal to the growth rate of the LDH coating, this may lead to a certain improvement in the corrosion resistance of the composite coating. This consequence may result from the LDH coating sealing the micropores on the MAO coating. For instance, Peng et al. [18] prepared a Mg–Al LDH coating on MAO-coated Mg alloy AZ31 surface using hydrothermal treatment with a pH of 12.8 at 120 °C for 12 h. The results show the corrosion current density, i_{corr} of the composite coating compared with the MAO coating is reduced from 9.45×10^{-6} A cm^{-2} to 3.92×10^{-6} A cm^{-2}, which indicates a small increase in corrosion resistance.

Thirdly, if the dissolution rate of the MAO coating is less than the growth rate of the LDH coating, the corrosion resistance of the composite coating will be improved. For example, Jiang et al. [28] fabricated a Mg–Al LDH coating on MAO-coated Mg alloy AZ91 surface

through a co-precipitation and hydrothermal at a pH of 11 and at a temperature of 120 °C. The result suggests the i_{corr} decreased from 1.27×10^{-6} A cm^{-2} for MAO coating to 1.03×10^{-7} A cm^{-2} for MAO-LDH coating, which shows a increased corrosion resistance.

If to obtain a composite coating with excellent corrosion resistance, the dissolution rate of the MAO coating must be by far slower than the growth rate of the LDH coating. Therefore, it is difficult to find the equilibrium point between the dissolution rate of the MAO coating and the growth rate of the LDH coating. Eliseev et al. [29] proposed that prior to the formation of LDH, $Mg(OH)_2$ layered structure and amorphous $Al(OH)_3$ agglomerates are preferentially deposited on Mg substrate surface, followed by LDH crystallization. Chen et al. [25] also found that the Mg substrate is preferentially dissolved; and $Mg_5(CO_3)_4(OH)_2 \cdot 5H_2O$ and $Al_5(OH)_{13}(CO_3) \cdot 5H_2O$ are formed before the formation of LDH due to the carbonate hydrolysis to form hydroxide. The scenario reveals that hydroxide may be the precursor for the formation of LDH. In our previous work, an extremely thin $Mg(OH)_2$ film was prepared using *in-situ* growth on MAO-coated Mg alloy AZ31 [30]. It is worth noting that it has a lower preparation temperature at 60 °C and a higher pH of 13.60. And the composite coating has good corrosion resistance, and its i_{corr} decreases three orders of magnitude than that of the substrate. This implies that the growth rate of the Mg$(OH)_2$ is greater than the dissolution rate of the MAO coating. Therefore, increasing the pH value and lowering the temperature may balance the dissolution rate of the MAO coating and the growth rate of the LDH coating to obtain a composite coating with excellent corrosion resistance.

In this study, it is hypothesized that the LDH coating can be prepared on MAO-coated Mg alloy AZ31 by adding an Al source to the original solution under the above preparation conditions [30]. And the corrosion resistance in simulated body fluids, cytotoxicity and formation mechanism of the MAO-LDH composite coating were explored.

2. Experimental

2.1. Materials

The as-extruded Mg alloy AZ31, cut into a cuboid with a dimension of 2 cm × 2 cm × 0.5 cm, was selected as the substrate. All chemicals were purchased from Qingdao Jingke Chemical Reagent Co., Ltd., China. Before the experiment, the substrates were ground with SiC sandpaper from 150 to 1500 grit, rinsed separately with distilled water and absolute ethanol, and dried with warm air.

2.2. Preparation of the MAO coating

MAO coatings were prepared using a device consisting of a HNMAO-20A-DPM400 power supply and a PMMA-made electrolytic cell equipped with a stainless-steel plate. Mg alloy AZ31 was regarded as the anode; and the stainless-steel plate as the cathode in MAO process. The electrolyte, solution A, consisted of 6 g L^{-1} phytic acid and 10 g L^{-1} NaOH. The frequency, duty cycle, current density, and oxidation time were fixed at 500 Hz, 20%, 83.3 mA cm^{-2}, and 3 min, respectively.

2.3. Preparation of the MAO-LDH composite coating

Solution B with a pH of 13.76 consisted of 40 g L^{-1} NaOH, 50 g L^{-1} EDTA-2Na and 5 g L^{-1} pure Al wire. Then, the MAO-coated substrates were placed in the solution B at 60 °C for 48 h. And a simple flow chart for preparation of the MAO-LDH coating was shown in Fig. 1.

2.4. Characterization of the coatings

The surface and cross-sectional morphologies of the MAO and MAO-LDH coatings were observed via field-emission scanning electron
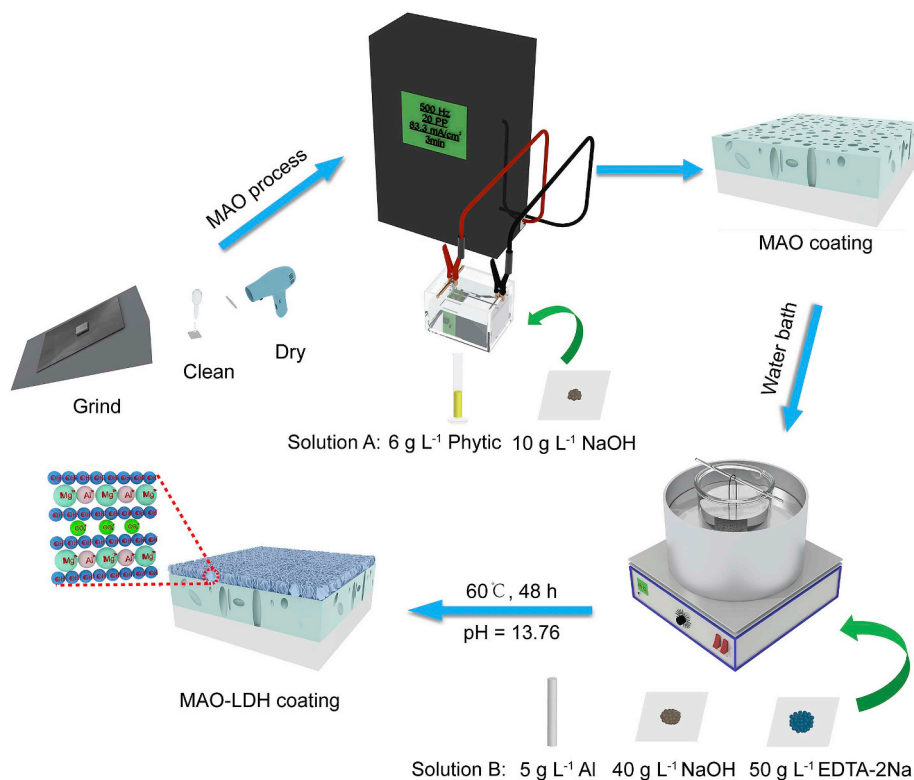
Fig. 1. Simple flow chart for preparation of the MAO-LDH coating.

microscopy (FE-SEM, Nova NanoSEM 450, US). And elemental compositions were detected using FE-SEM attached energy dispersive X-ray spectrometry (EDS) device. Chemical functional groups of the coatings were analyzed through Fourier transform infrared spectrometry (FT-IR, Nicolet 380, Thermo Electron Corporation, US) in the wavenumber range from 4000 to 400 cm^{-1} with a resolution of 1 cm^{-1}. Crystallographic structure was detected through an X-ray diffractometer (XRD, Rigaku D/MAX2500PC, Japan) with a Cu target (λ = 0.154 nm) from 5° to 80° over 2θ range at a scanning rate of 8° min^{-1}. Chemical compositions of the MAO-LDH coating was also revealed via X-ray photoelectron spectroscopy (XPS, ESCALAB250, Thermo VG Co, East Sussex, US) with an Al Kα X-ray source.

2.5. Corrosion characterization

The corrosion resistance of the Mg alloy AZ31 substrate, MAO coating, and MAO-LDH coating were evaluated via potentiodynamic polarization curves and electrochemical impedance spectroscopy (EIS) using an electrochemical device (VersaSTAT 4, USA). A conventional three-electrode cell included that a sample was used as the working electrode, a saturated calomel electrode (SCE) as the reference electrode, and a platinum electrode as the counter electrode. The samples were placed into Hank's solution (8.0 g L^{-1} NaCl, 1.0 g L^{-1} $C_6H_6O_6$ (Glucose), 0.35 g L^{-1} $NaHCO_3$, 0.4 g L^{-1} KCl, 0.14 g L^{-1} $CaCl_2$, 0.1 g L^{-1} $MgCl_2{\cdot}6H_2O$, 0.06 g L^{-1} $MgSO_4{\cdot}7H_2O$, 0.06 g L^{-1} KH_2PO_4 and 0.06 g L^{-1} $Na_2HPO_4{\cdot}12H_2O$) at room temperature. The potentiodynamic polarization curves were obtained at a scan rate of 2 mV s^{-1}. The EIS test was carried out from 10 kHz to 0.01 Hz with an interference potential of 10 mV. The hydrogen evolution test was also employed to evaluate the long-term corrosion resistance. The device consisted of a funnel connected to an acid burette inverted in a beaker. The samples were placed under a funnel containing the Hank's solution at 37.5 ± 0.1 °C. The solution scale in the burette was recorded intermittently. Three parallel samples in each group were tested.

2.6. Cytocompatibility tests

2.6.1. Cell proliferation assay

Mouse MC3T3-E1 pre-osteoblasts were placed in 10% fetal bovine serum (FBS) and 1% penicillin-streptomycin solution modified medium (α-DMEM) in a humidified atmosphere with 5% CO_2 at 37 °C for *in vitro* cell culture testing. An indirect contact method to culture cells using 100% alloy extract was used to assess biocompatibility. Prior to testing, each side of all samples on was sterilized using UV for 6 h. Then, the extracts were prepared in a ratio of the sample surface area to the extraction medium (α-DMEM) of 1 mL cm^{-2} in a humidified atmosphere with 5% CO_2 at 37 °C for 3 d. Next, the seeded cells were cultured on a 96-well plate at a density of 5000 cells per well for 24 h to allow attachment. Furthermore, the medium was replaced using 100 μL of α-DMEM supplemented with 100% extracts and 10% FBS. After culturing for different times (1, 3 and 5 days), each well was added another solution to replace the extract using fresh medium and 10 μL of 3-(4,5-dimethylthiazol-2-yl)-2,5-diphenyltetrazolium bromide (MTT, M8180, Solarbio, China). After 4 h of incubation, blue formazan crystals were formed and dissolved through dimethyl sulfoxide (DMSO). Finally, the absorbance was measured using a microplate reader (Multiskan Go 1510, Thermo Fisher Scientific, China) at a wavelength of 492 nm. And cell viability was calculated according to Ref. [31].

2.6.2. LIVE/DEAD activity measurement

Osteoblasts were cultured on a 96-well plate at a density of 5000 cells per well for 24 h. The cell culture medium in each well was replaced with 500 μL of 100 vol% extract mediums. After the cells were cultured in a humidified atmosphere with 5% CO_2 at 37 °C for 1 d, cells were stained through LIVE/DEAD® assay (L3224, Invitrogen, China). That is, a mixed solution of Calcein-AM and Ethidium homodimer was added to each well and incubated for 30 min. Cells were observed through fluorescence microscopy (EVOS, Invitrogen, China), in which live and dead cells were stained green and red, respectively. Cells cultured in fresh medium without samples were used as negative controls
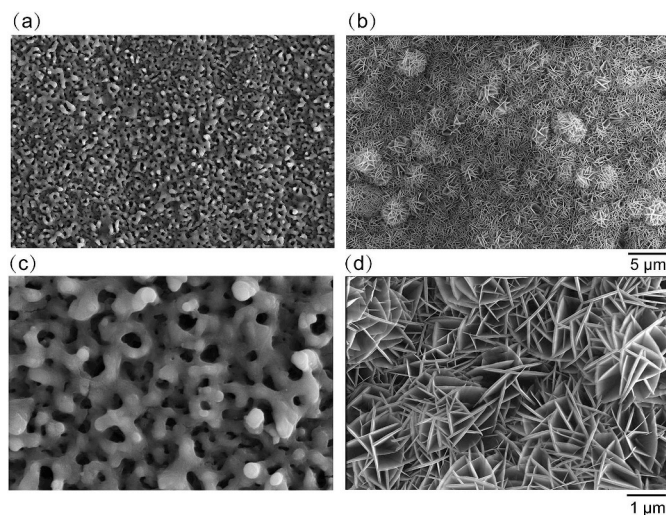
Fig. 2. Surface morphology images of the (a, c) MAO, and (b, d) MAO-LDH coatings.

with three replicates per sample.

2.7. Statistical analysis

Statistical analysis was carried out via the independent-samples *t*-test. Differences were considered significant at *$*P < 0.05$* or *$**P < 0.01$*. All the experiments were executed three times, with three replicates in each test.

3. Results

3.1. Characteristics of the surface and cross-sectional of the coatings

The surface morphology images of the (a, c) MAO, and (b, d) MAO-LDH coatings are displayed in Fig. 2. As can be observed from Fig. 2a and c, the MAO coating has a typical porous morphology with micro-cracks. The MAO coating was completely covered by a layer of na-nosheet structured LDH in Fig. 2b and d. However, the overall surface of the LDH coating is not smooth, which may be due to the porous and rough structure of the MAO surface.

Fig. 3 shows the element compositions of the corresponding coat-ings detected using EDS. Elemental P is detected in the MAO coating, which implies that phytic acid participates in the formation of MAO
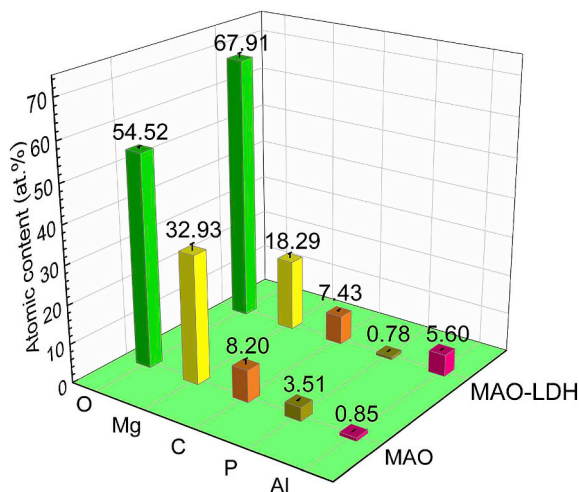

Fig. 3. Element composition of the MAO and MAO-LDH coatings.

coating, while the elemental C may come from CO_2 in the air [32] besides phytic acid. The MAO-LDH coating shows lower content of elemental Mg and P and higher content of elemental Al and C. This finding indicates that the MAO coating is covered by the LDH coating; and Al^{3+} is adsorbed and participates in the formation of the LDH. Notably, the Mg/Al atomic ratio is approximately 3:1, which is con-sistent with Mg/Al atomic ratio in Mg–Al LDH crystal structure [17,33].

Fig. 4 demonstrates the cross-sectional views of the (a) MAO, and (b, c) MAO-LDH coatings. And the corresponding mapping images of (d) Mg, (e) P and (f) Al elements for MAO-LDH coating are also shown in Fig. 4. The thickness of the MAO coating is 5.60 ± 0.43 μm, which exhibits a porous structure and a non-uniform thickness, whereas the thickness of the MAO-LDH coating is 7.83 ± 0.47 μm. It is worth noting that the thickness of the LDH coating is 3.83 ± 0.62 μm, while the MAO coating decreased to only 4.00 ± 1.08 μm. As can be observed from the mapping images of the MAO-LDH coating, the elemental Al and P have an intersect section. The reason is that the MAO coating is partially dissolved, and Al^{3+} in the solution permeates into the MAO coating through micropores during the preparation process of the LDH coating. In addition, the higher concentration of Al in local areas in the substrate in Fig. 4f discloses the presence of Al–Mn phase [34].

The XRD patterns of the (a) Mg alloy AZ31 substrate, (b) MAO coating, and (c) MAO-LDH coating are shown in Fig. 5. The char-acteristic peaks of α-Mg are observed in all samples, while the MAO coating also has another characteristic peak of MgO. In particular, the element P is detected in the MAO coating according to the EDS results of Fig. 3. However, the characteristic peak of P is not observed due to the trace of P-bearing crystalline. It is worth noting that the char-acteristic peaks of $Mg_6Al_2(CO_3)(OH)_{16} \cdot 4H_2O$ are observed in the MAO-LDH coating, which implies successful preparation of the Mg–Al LDH.

Fig. 6 illustrates the FT-IR spectra of the (a) MAO and (b) MAO-LDH coatings. The Mg–O bonds correspond to MgO, which is in concordance with the result of the XRD. For MAO-LDH coating, absorption peaks of 3726, 3418, 1612 cm^{-1} designate the stretching vibration of H–O–H and the symmetric stretching from the water molecule O–H. That in-dicates that water molecules exist in the MAO-LDH coating. The peaks of 1359, 783, 552 cm^{-1} correspond to the asymmetric stretching CO_3^{2-} in the carbonate molecule, which implies that the anions in LDH are in the form of CO_3^{2-}. And the absorption band of 2990 cm^{-1} corresponds to CO_3^{2-}-H_2O, which confirms that CO_3^{2-} bonds H_2O molecules through hydrogen bonding in the hydrotalcite interlayer. The results disclose that CO_3^{2-} intercalated Mg–Al LDH coating is suc-cessfully prepared on MAO-coated Mg substrate through water bath treatment at 60 °C with a pH of 13.76.

3.2. Corrosion behaviors

The results of EIS of the (I) Mg alloy AZ31 substrate, (II) MAO coating, and (III) MAO-LDH coating are demonstrated in Fig. 7. The greater the impedance modulus, |Z|, at low frequency is, the better the corrosion resistance is. As can be seen from in Bode plot (Fig. 7a), the |Z| value of the Mg alloy AZ31 substrate is 478.03 Ω cm^2, lower than that of the MAO coating (9.46×10^4 Ω cm^2), and by far lower than that of the MAO-LDH coating (3.45×10^6 Ω cm^2). The increasing order of corrosion resistance of the samples is: MAO-LDH coating > MAO coating > Mg alloy AZ31 substrate. Moreover, the MAO-LDH coating exhibits at least two-time constants, corresponding to the multilayer structure from Bode phase angle plot (Fig. 7b). The phase angle of the intermediate frequency range becomes flatter and smoother, which indicates that the MAO-LDH coating is denser and more uniform. Fur-thermore, Fig. 7 also illustrates Nyquist plots of the (c) Mg alloy AZ31 substrate, (d) MAO coating, and (e) MAO-LDH coating. Large im-pedance loop at low frequency represents greater corrosion resistance. In Fig. 7e, the MAO-LDH coating has the largest semicircle diameter, which indicates the best corrosion resistance.

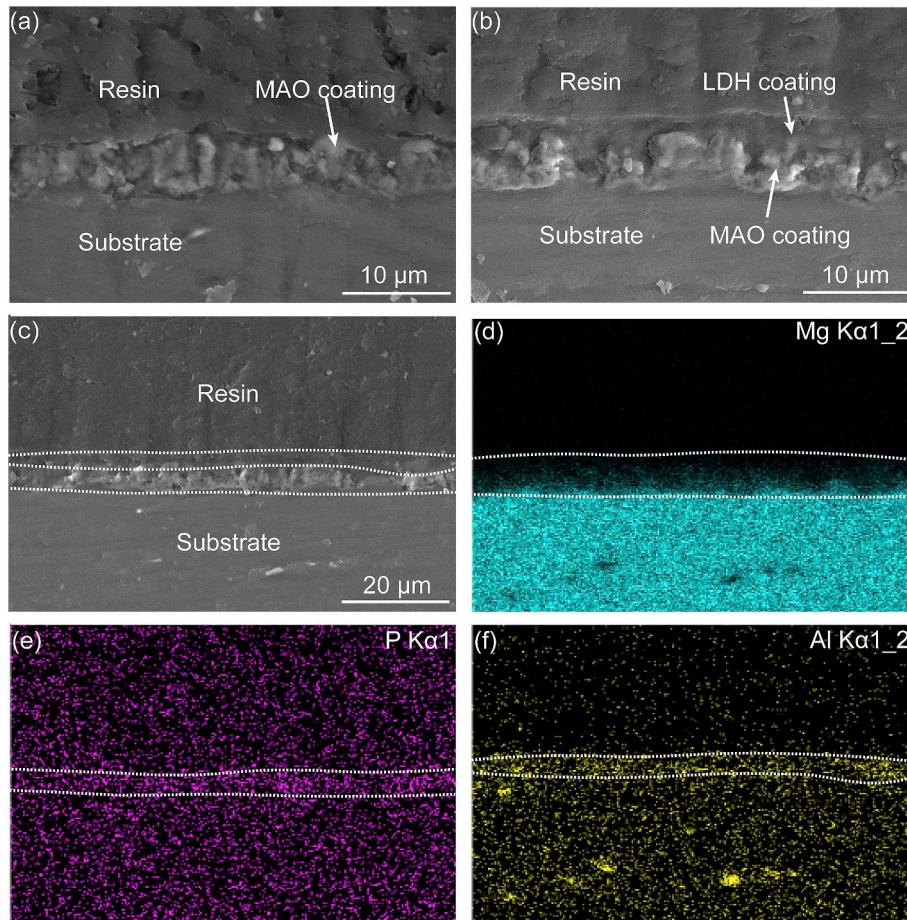The corresponding equivalent circuits (ECs) of the Mg alloy AZ31

Fig. 4. Cross-sectional views of the (a) MAO, and (b, c) MAO-LDH coatings; and corresponding EDS mapping images of (d) Mg, (e) P and (f) Al elements for the MAO-LDH coating.
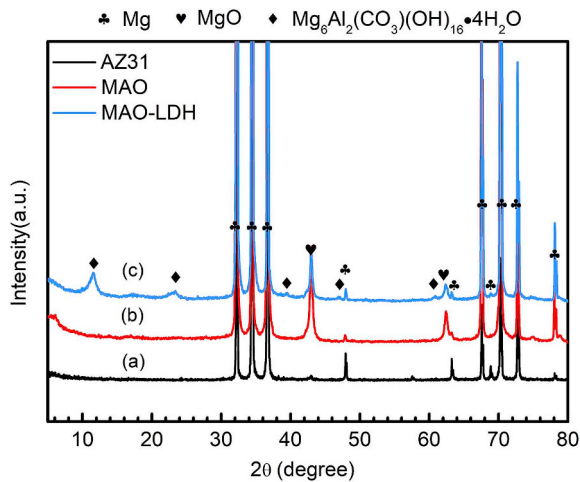

Fig. 5. XRD patterns of the (a) Mg alloy AZ31 substrate, (b) MAO coating, and (c) MAO-LDH coating.

Fig. 6. FT-IR spectra of the (a) MAO and (b) MAO-LDH coatings.

substrate, MAO coating, and MAO-LDH coating are shown in Fig. 7f–h. The fitting results are presented in Table 1. R_s and R_{ct} represent the solution resistance and charge transfer resistance in the ECs, respectively. CPE_1 and CPE_2 represent constant phase components, whereas CPE_3 represents double layer capacitance. C_1 signifies the capacitance of the corresponding coating. R_1 and R_2 symbolize the resistance of the corresponding coating. As can be seen from Fig. 7f, the high-frequency region consists of CPE_1 and R_{ct}, indicating that the loose porous
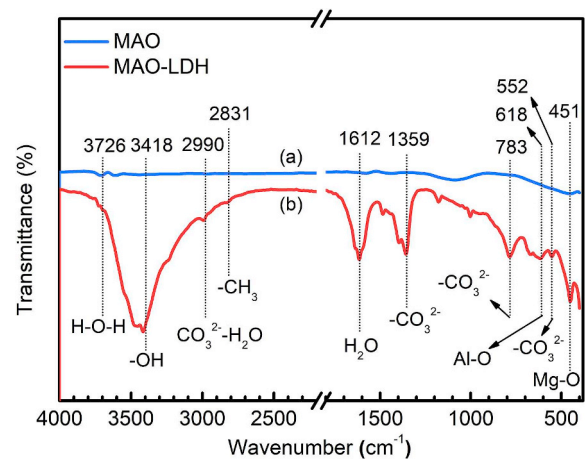
corrosion product film on the Mg substrate. The low-frequency region is composed of the inductance (L) and resistance (R_L), implying the pitting corrosion of the Mg substrate. The MAO coating consists of the resistance (R_1) and constant phase component (CPE_1). For the MAO-LDH coating, R_1 and CPE_1 corresponds to the out-layer LDH coating; R_2 and CPE_2 corresponds to the inter-layer MAO coating; R_{ct} and CPE_3 represent charge transfer resistance and double layer capacitance. Z_w represents the diffusion resistance of the LDH coating, which confirms that the LDH coating has an ion-exchangeable ability. The larger the R_{ct} value reflects the better the corrosion resistance. Results of the R_{ct}
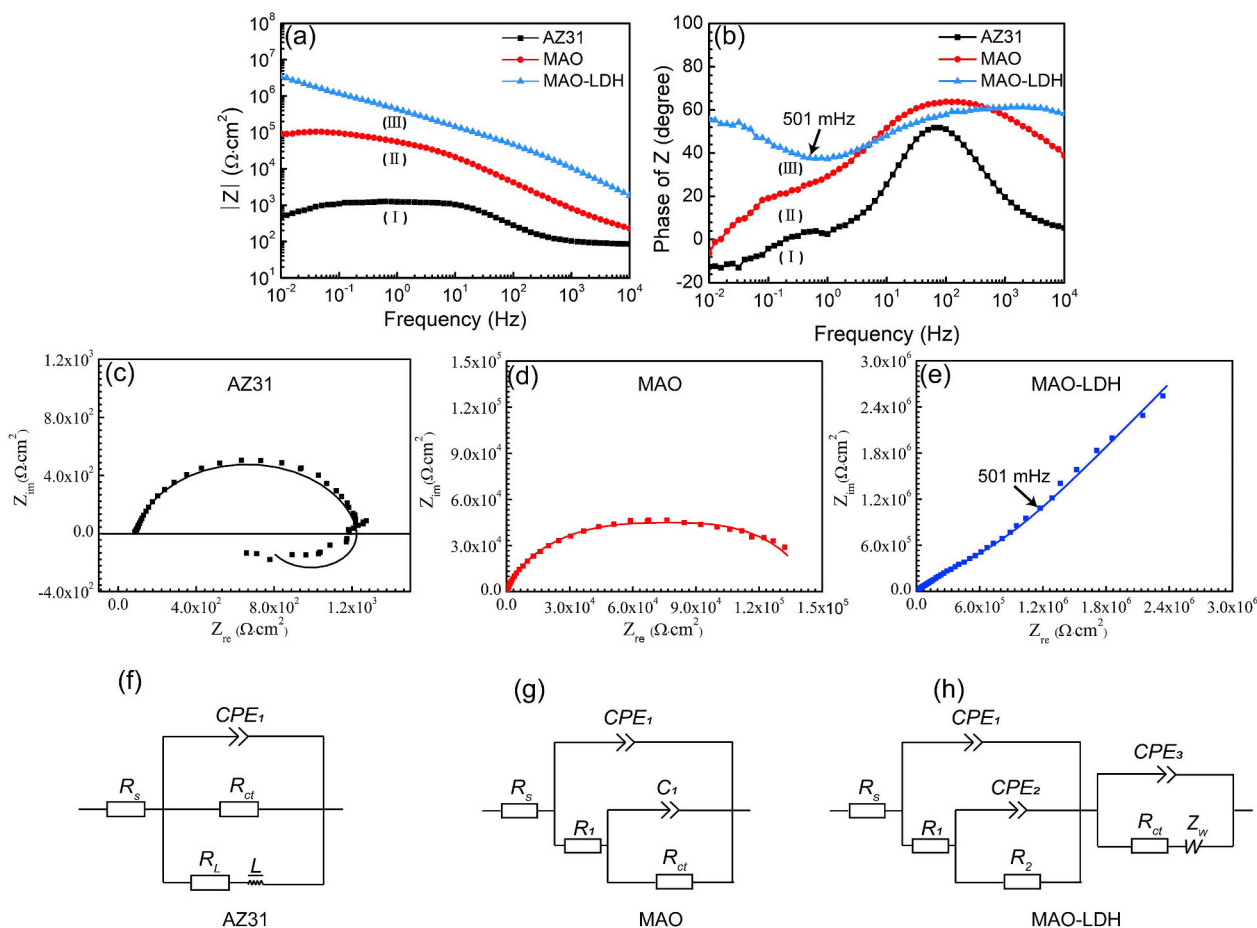
Fig. 7. (a) Bode and (b) Bode phase angle plots of the (I) Mg alloy AZ31 substrate, (II) MAO coating and (III) MAO-LDH coating. Nyquist plots (c–d) and the corresponding electrical equivalent circuit models (f–h) of all samples.

Table 1
Electrochemical data obtained via equivalent circuit fitting of EIS curves.

Samples	Mg alloy AZ31	MAO	MAO-LDH
R_s (Ω cm^2)	8.82×10^1	4.01×10^1	3.83×10^1
R_1 (Ω cm^2)	–	1.08×10^5	6.05×10^4
R_2 (Ω cm^2)	–	–	1.21×10^6
R_L (Ω cm^2)	1.60×10^3	–	–
R_{ct} (Ω cm^2)	1.15×10^3	3.53×10^4	3.85×10^6
CPE_1 (Ω^{-1} s^n cm^{-2})	1.32×10^{-5}	1.90×10^{-7}	8.46×10^{-8}
CPE_2 (Ω^{-1} s^n cm^{-2})	–	–	2.49×10^{-6}
CPE_3 (Ω^{-1} s^n cm^{-2})	–	–	1.48×10^{-7}
C_1 (F cm^{-2})	–	1.17×10^6	–
Z_W ($\Omega^{-0.5}$ s^{-1} cm^{-2})	–	–	5.83×10^{-7}
n_1	8.83×10^{-1}	8.38×10^{-1}	7.93×10^{-1}
n_2	–	7.00×10^{-1}	5.16×10^{-1}
n_3	–	–	8.15×10^{-1}
Chi-Squared	4.13×10^{-3}	5.21×10^{-4}	1.65×10^{-4}

values in Table 1 can be ranged in the following order: Mg alloy AZ31 substrate ($1.15 \times 10^3 \ \Omega \ $cm^2) < MAO coating ($3.53 \times 10^4 \ \Omega \ $cm^2) < MAO-LDH coating ($3.85 \times 10^6 \ \Omega \ $cm^2). This shows the MAO-LDH coating can provide a best protection for the substrate.

Fig. 8a and b correspond to potentiodynamic polarization curves and the fitting results of the i_{corr} and corrosion potential (E_{corr}) of the (I) Mg alloy AZ31, (II) MAO coating, and (III) MAO-LDH coating. As can be observed from Fig. 8a-(III), in the cathode region, the MAO-LDH coating has a lowest cathode current density, which implies that the composite coating effectively inhibits the cathodic hydrogen evolution reaction, whereas, in the anode region, the MAO-LDH coating with the

lowest anode current density indicates that the dissolution of the anode α-Mg is suppressed. Also, the MAO-LDH coating in the anode region exhibits a significant shift of the breakdown potential in the positive direction and a larger passivation region, similar to the passive current density region present in bare steel [35–38]. This scenario may be due to the anion exchange behavior of the LDH coating as mentioned in the introduction. This result demonstrates that Cl$^-$ ions have few active sites on the surface of the MAO-LDH coating due to the difficulty to be adsorbed [39,40]. These lead to that Cl$^-$ induced pitting is delayed. Therefore, the breakdown potential, that is, pitting potential, is enhanced. The higher pitting potential represents stronger pitting resistance. Moreover, after the first breakdown of the MAO-LDH coating, a phenomenon of breakdown-re-passivation-re-breakdown is found, which implies that the coating is repaired again after the coating is destroyed, that is, it has a self-healing ability [17]. According to previous research in our group [17,21], this is due to the diffusion behavior of the LDH coating. At the pitting site, the intercalated CO_3^{2-} diffuses to the surface layer and combines with the dissolved Mg^{2+} to form $MgCO_3$. However, $MgCO_3$ converted to a lower solubility $Mg(OH)_2$ in an alkaline environment, which deposits and covers at the pitting site to achieve film repair. According to the result of Fig. 8d, the i_{corr} values of the samples can be ranged in decreasing order: Mg alloy AZ31 (1.28×10^{-5} A cm^{-2}) > MAO coating (3.94×10^{-7} A cm^{-2}) > MAO-LDH coating (6.81×10^{-9} A cm^{-2}). The smaller value of i_{corr} is, the better the corrosion resistance gets. The results imply that the MAO-LDH coating has the best corrosion resistance.

Fig. 9a shows the hydrogen evolution rate curves of all samples immersing in the Hank's solution for 154 h. At the initial stage of
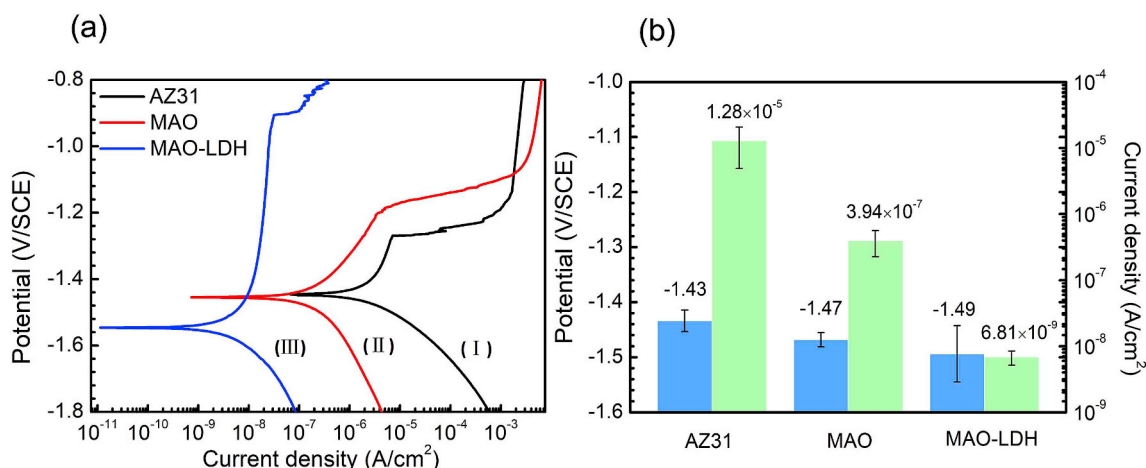
Fig. 8. (a) Potentiodynamic polarization curves and (b) corresponding i_{corr} and E_{corr} of the (I) Mg alloy AZ31 substrate, (II) MAO coating, and (III) MAO-LDH coating.

immersion (I), the hydrogen evolution rate of Mg alloy AZ31 substrate rises rapidly and then gradually decreases. This is because α-Mg is first corroded, and then corrosion product ($Mg(OH)_2$) film is formed on the substrate surface, which can inhibit the corrosion. The hydrogen evolution rates of the MAO and MAO-LDH coatings are relatively gentle.

After soaking for 20 h (II), the hydrogen evolution rates of all samples increased. For the Mg alloy AZ31 substrate, the corrosion product is dissolved and thus fresh surface is again exposed to the Hank's solution. For the MAO and MAO-LDH coatings, the reason may be the occurrence of the pitting or localized corrosion, which results in partial coating
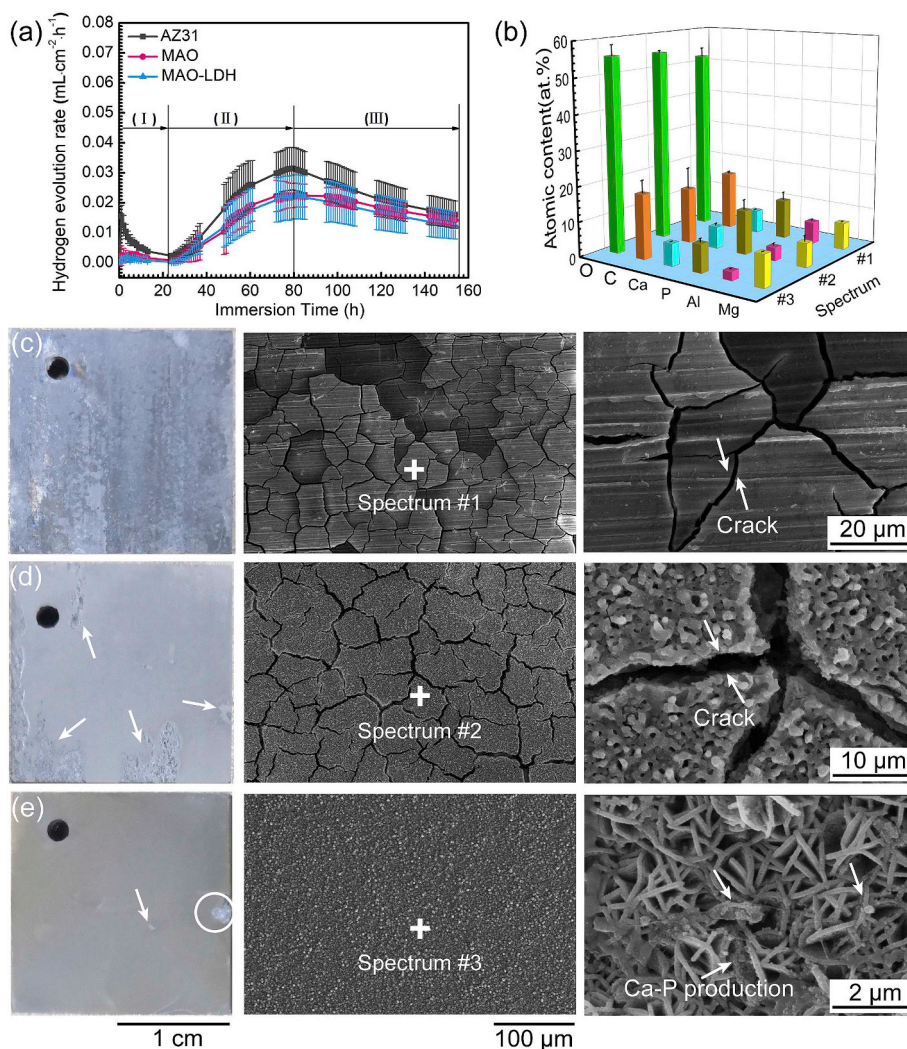

Fig. 9. (a) Hydrogen evolution rates, (b) element compositions, and digital camera photographs and SEM images of the (c) Mg alloy AZ31 substrate, (d) MAO coating, and (e) MAO-LDH coating in Hank's solution for 154 h.

failure. As the soaking time increased (III), the hydrogen evolution rates gradually decrease, which implies a new corrosion product film is formed at the exposed portion of the substrate. In general, MAO-LDH coating always has a lower hydrogen evolution rate than that of the MAO coating and substrate, which indicates it can provide a better protection for the substrate.

Fig. 9 also demonstrates the corresponding element compositions (b) and digital camera photographs and SEM images of the (c) Mg alloy AZ31 substrate, (d) MAO coating, and (e) MAO-LDH coating in Hank's solution for 154 h. As can be observed from Fig. 9c, the surface of the substrate appears damaged and becomes rough. And dry riverbed morphology is also observed. For the MAO coating, large localized corrosion and many large cracks are observed, whereas localized corrosion, that is, pitting corrosion is rarely found on the MAO-LDH coating. The MAO-LDH coating remains intact without cracking; and the nanosheet structured morphology of the LDH coating is maintained, which shows that the corrosion is very slight. The results confirm that the reason for the increase in the hydrogen release rate in the second stage of the hydrogen evolution rate curve is the pitting or localized corrosion of the surface of the MAO and MAO-LDH coatings. From the result of the EDS (Fig. 9b), elements Ca and P are detected on all samples surface. Also, the Ca/P ratios of the Mg alloy AZ31 substrate, MAO coating and MAO-LDH coating are 0.58, 0.50 and 0.80, respectively. The MAO-LDH coating has the highest Ca/P ratio. And obviously, Ca–P corrosion products are observed on the nanosheet structured LDH, which seals part pores of the LDH coating. However, the MAO coating has the lowest Ca/P ratio, which is due to the presence of the high content of P in MAO coating. Generally, the MAO-LDH coating has the lowest hydrogen evolution rate and rarely localized corrosion than that of the others, which provides a better protection for the substrate. And nanosheet structured LDH is more conducive to the formation of Ca–P products, which may be beneficial to the growth of osteoblasts.

3.3. Cytotoxicity tests

As bone implant materials, Mg alloys should have controllable degradation rate and good biocompatibility in orthopedic or cardiovascular surgical applications [41]. In this study, an indirect contact method to culture cells using alloys extract is used to assess biocompatibility. Fig. 10 demonstrates (a) OD values and (b) cell viability of MC3T3-E1 cells cultured in 100% alloy extracts of the Mg alloy AZ31 substrate, MAO coating, and MAO-LDH coating for 1, 3 and 5 days. Once cell viability is above 75%, this result indicates the non-toxicity to the cells [42,43]. As can be observed from Fig. 10b, the MAO-LDH group shows more than 90% cell viability during 1, 3, and 5 days of incubation, which implies that it is non-toxic to the cells. Also, the high concentration of the extracts (50%, 75% and 100%) has an adverse effect on cell viability of the cells; and the content of 25% of the extracts is beneficial for cell survival [44]. Thus, when 100% alloy extracts show more than 90% cell viability, further indicating that the MAO-LDH coating is non-toxic to the cells. The MAO-LDH group has higher cell viability than others group, which indicates a better biocompatibility. Live/dead staining of MC3T3-E1 post seeding for 24 h is shown in Fig. 10c–f. The osteoblasts of all samples exhibit a diffuse morphology of flat spindle and filopodia, which imply good cell spreading and positive affinity for the cells. The results disclose that the MAO-LDH group exhibits acceptable and enhanced cytocompatibility to osteoblasts.

4. Discussion

4.1. Growth mechanism of the MAO-LDH coating

Our previous studies have discussed the growth mechanism of Mg (OH)$_2$ on MAO coatings [30]. The dissolution of α-Mg matrix occurs near the Al–Mn phases, leads to the formation of Mg(OH)$_2$. In this experiment, an Al source is added into the original solution to prepare the LDH coating. Therefore, the growth process of the LDH coating may conclude the adsorption of Al^{3+} and the partial substitution of Mg^{2+} on the layer by Al^{3+} isomorphism. To further confirm our hypothesis, the MAO-coated Mg alloys were soaked in solution B for different times (1 min, 10 min, 1 h, 6 h, 12 h, and 24 h) to observe the growth of LDH coating.

4.1.1. Change in surface morphology

SEM images of the MAO-LDH coatings at various soaking time are displayed in Fig. 11. And chemical compositions of the MAO-LDH coatings at various soaking time are illustrated in Fig. 12. In the first stage (1 min of immersion), tiny isolated coating is formed on the MAO surface (Fig. 11a). Furthermore, the content of Al and manganese (Mn) at spectrum #1 is higher than that of spectrum #2 (Fig. 12), which indicates that the presence of Al–Mn phase at spectrum #1, also
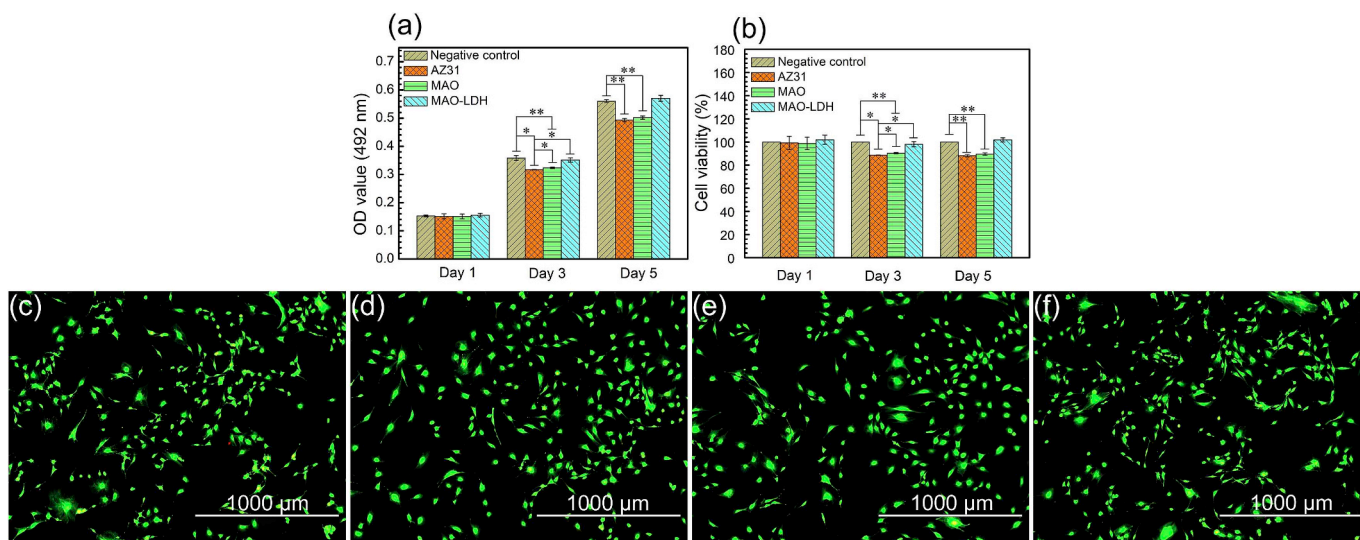

Fig. 10. OD values (a) and Cell viability (b) of MC3T3-E1 cultured in different extracts prepared with the negative control, Mg alloy AZ31 substrate, MAO coating, and MAO-LDH coating for 1, 3 and 5 days. Statistically significant differences (*$P < 0.05$, **$P < 0.01$.); Fluorescent images (c–f) of MC3T3-E1 after culturing for 24 h in extracts of the (c) negative control, (d) AZ31 substrate, (e) MAO coating and (f) MAO-LDH coating.
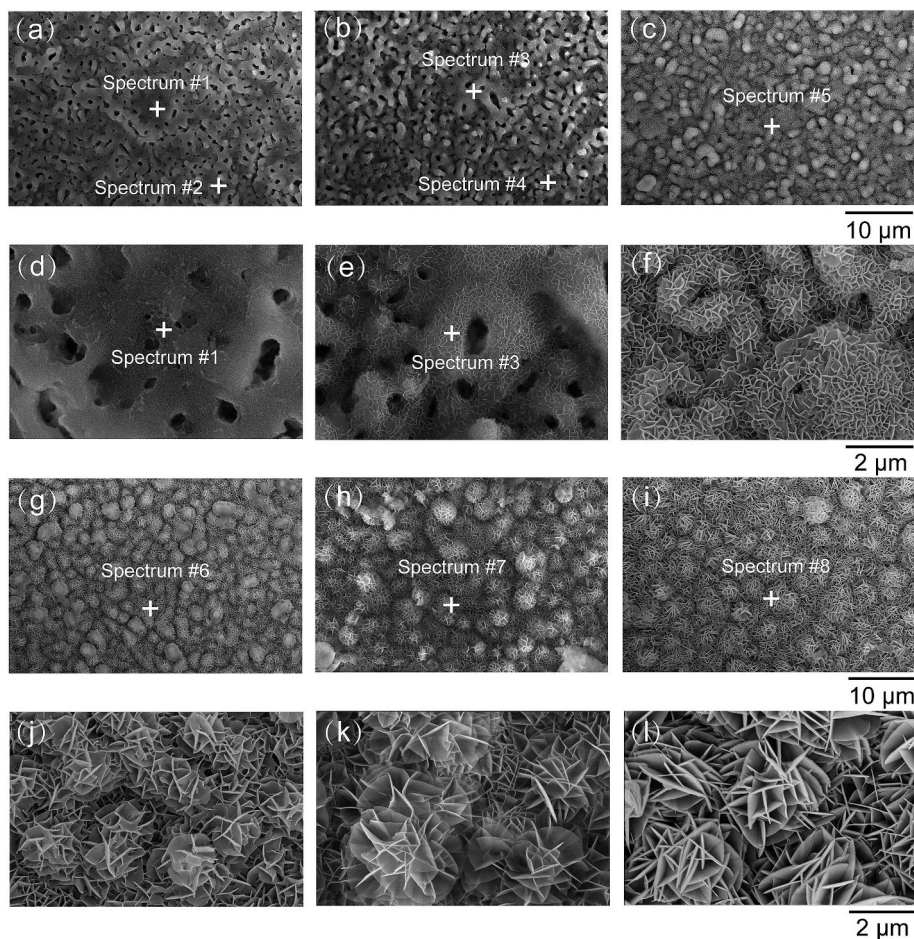
Fig. 11. SEM images of MAO-LDH coatings at various soaking time: 1 min (a, d), 10 min (b, e), 1 h (c, f), 6 h (g, j), 12 h (h, k) and 24 h (i, l).
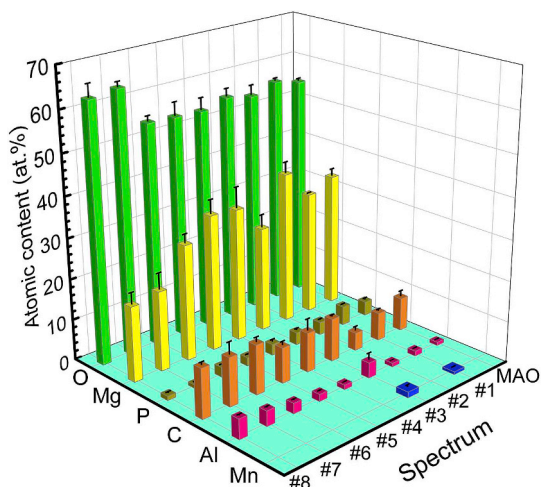

Fig. 12. Element compositions of the MAO-LDH coatings at various soaking time.

marking that the coating initiates near the Al–Mn phase. In other word, the higher potential Al–Mn phase acts as the cathode, and the lower potential α-Mg matrix acts as the anode, resulting in preferential dissolution of α-Mg near the Al–Mn phase and adsorption of OH^- to form the $Mg(OH)_2$ precipitates.

And the anode reaction followed as:

$$Mg \rightarrow Mg^{2+} + 2e^- \tag{1}$$

Cathodic reaction:

$$2H_2O + 2e^- \rightarrow 2OH^- + H_2\uparrow \tag{2}$$

Overall reaction:

$$Mg + 2H_2O \rightarrow Mg(OH)_2 + H_2\uparrow \tag{3}$$

Moreover, MgO on the MAO surface adsorbs free OH^- ions and gradually converted to $Mg(OH)_2$.

$$MgO + H_2O \rightarrow Mg(OH)_2 \tag{4}$$

In the second stage (10 min of immersion), as $Mg(OH)_2$ sheet structure grows, Al^{3+} ions begin to be adsorbed to the MAO surface, which could be confirmed though the higher Al content at spectrum #4 than that of spectrum #2 in Fig. 12f. When the Al^{3+} ions are adsorbed, the LDH crystals may form on the surface of the MAO coating. In the third stage (after 1 h of immersion), nanosheet structured LDH coating continues to grow, from small to large, with accompanied by a large amount of Al^{3+} deposition. Finally, an LHD coating with thicker and larger sheet structure is formed on the surface of MAO coating with time. The results show the nanosheet structured LDH coating rapidly grows and quickly covers the surface of the MAO coating. Moreover, during the initial soaking period, the surface of the MAO coating keeps intact and no significant dissolution is observed. This confirms that a high pH and a low preparation temperature balance the dissolution rate of the MAO coating and the growth rate of the LDH coating.

4.1.2. Change in crystallographic structure

Fig. 13 indicates the XRD patterns of the immersion at different time. The diffraction peak of the LDH is not observed on the MAO coated Mg alloy as soaked for 1 min (Fig. 13a). A weak diffraction peak
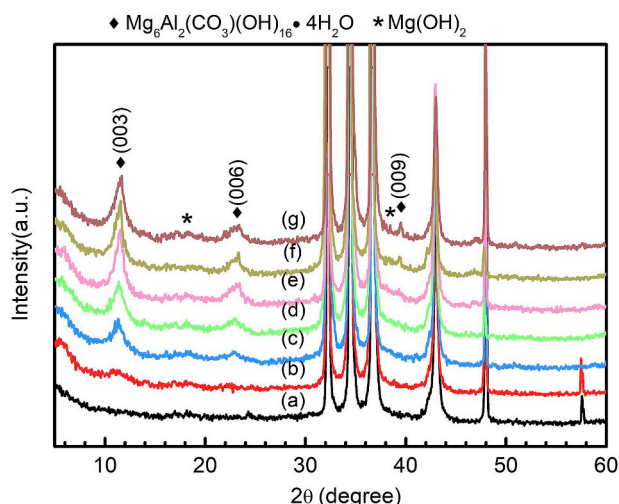
Fig. 13. XRD spectrums of the MAO-LDH coatings at various soaking time: 1 min (a), 10 min (b), 1 h (c), 6 h (d), 12 h (e), 24 h (f), and 48 h (g).

of the LDH is observed as immersed for 10 min (Fig. 13b), which confirms that LDH crystals begin to form. As the soaking time increases, the intensity of the diffraction peaks of the LDH increases, which manifests that the LDH crystallinity increases. In addition, the very weak diffraction peak of $Mg(OH)_2$ is observed on the MAO coated Mg alloy as soaked for 1 min (Fig. 13a), which indicates that the formation of $Mg(OH)_2$ is preferentially fast than LDH. However, the diffraction peak of $Al(OH)_3$ is not observed at the beginning of the immersion,

probably because the content was too low.

4.1.3. Change in elemental Al

In order to further explore the LDH formation process, MAO-coated Mg alloys immersed for different time are analyzed using XPS. And the peak fit of elemental Al is applied to analyze the change of Al content on the surface of the MAO coating. Fig. 14 shows the curve fitting of high-resolution Al 2p peaks of the MAO-coated Mg alloys immersed for different time. In Fig. 14a, the surface of the MAO coating has only Al_2O_3, which is derived from the oxidized Al in Mg alloy AZ31 during MAO process. After soaking for 1 min (Fig. 14b), $Al(OH)_3$ is observed on MAO surface, which confirms that Al^{3+} are adsorbed and combined with OH^- to form $Al(OH)_3$, also indicating that the formation of Al $(OH)_3$ is quicker than that of LDH. The reaction was as follows:

$$Al^{3+} + 3OH^- \rightarrow Al(OH)_3 \tag{5}$$

When immersed for 10 min (Fig. 14c), the LDH coating is observed on the surface of the MAO coating, which is consistent with the results of XRD. At the initial stage of immersion, it is considered that the content of Al $(OH)_3$ generated on the surface of the MAO coating is much lower than that of $Mg(OH)_2$. Therefore, the formation mechanism of LDH is more likely resulted from partial Mg^{2+} ions in $Mg(OH)_2$ replaced by Al^{3+} ions in the presence of CO_3^{2-} ions. The chemical reactions are as follows [25,33].
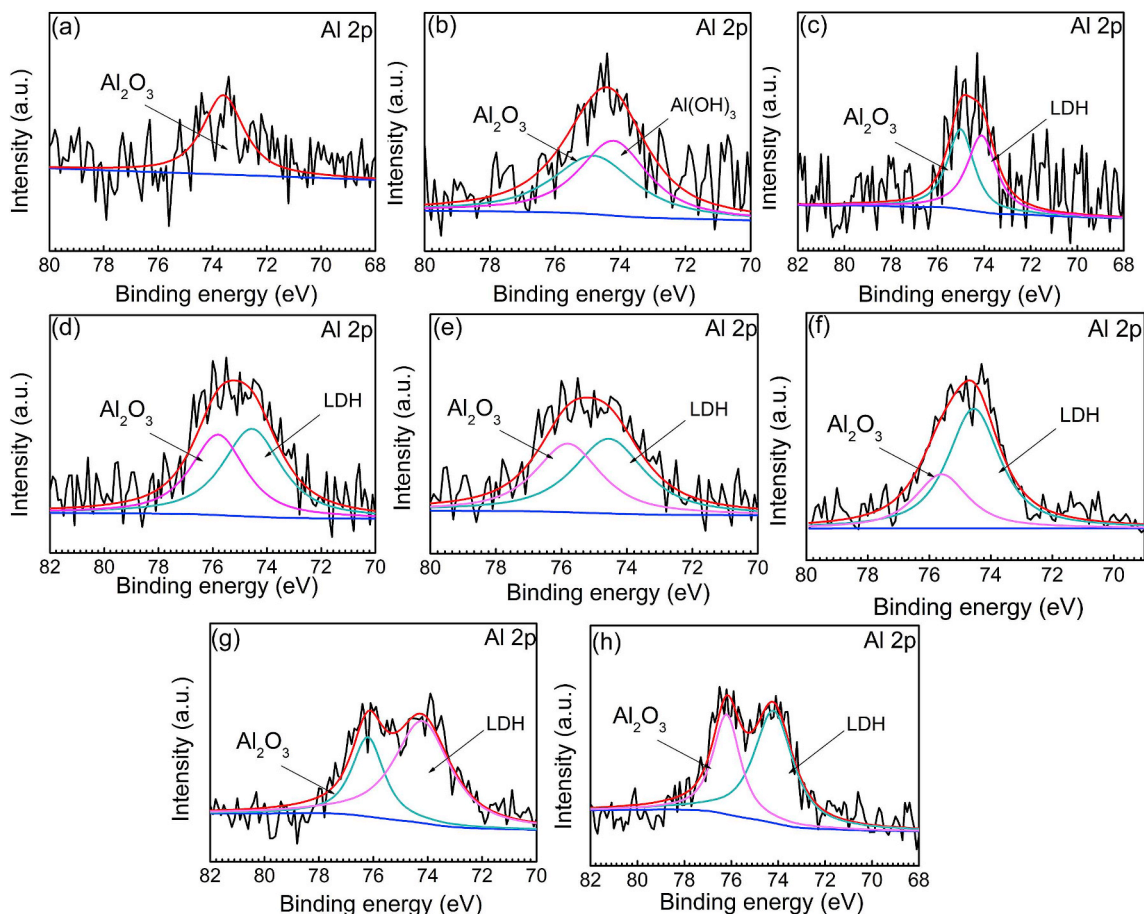
$$CO_2 + H_2O \rightarrow CO_3^{2-} + 2H^+ \tag{6}$$

$$2Mg(OH)_2 + Al^{3+} + 3OH^- \rightarrow Mg_2Al(OH)_7 \tag{7}$$
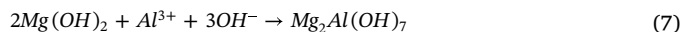

Fig. 14. XPS spectrums of the peak of Al 2p of the MAO-LDH coatings at various soaking time: 0 min (a), 1 min (b), 10 min (c), 1 h (d), 6 h (e), 12 h (f), 24 h (g), and 48 h (h).
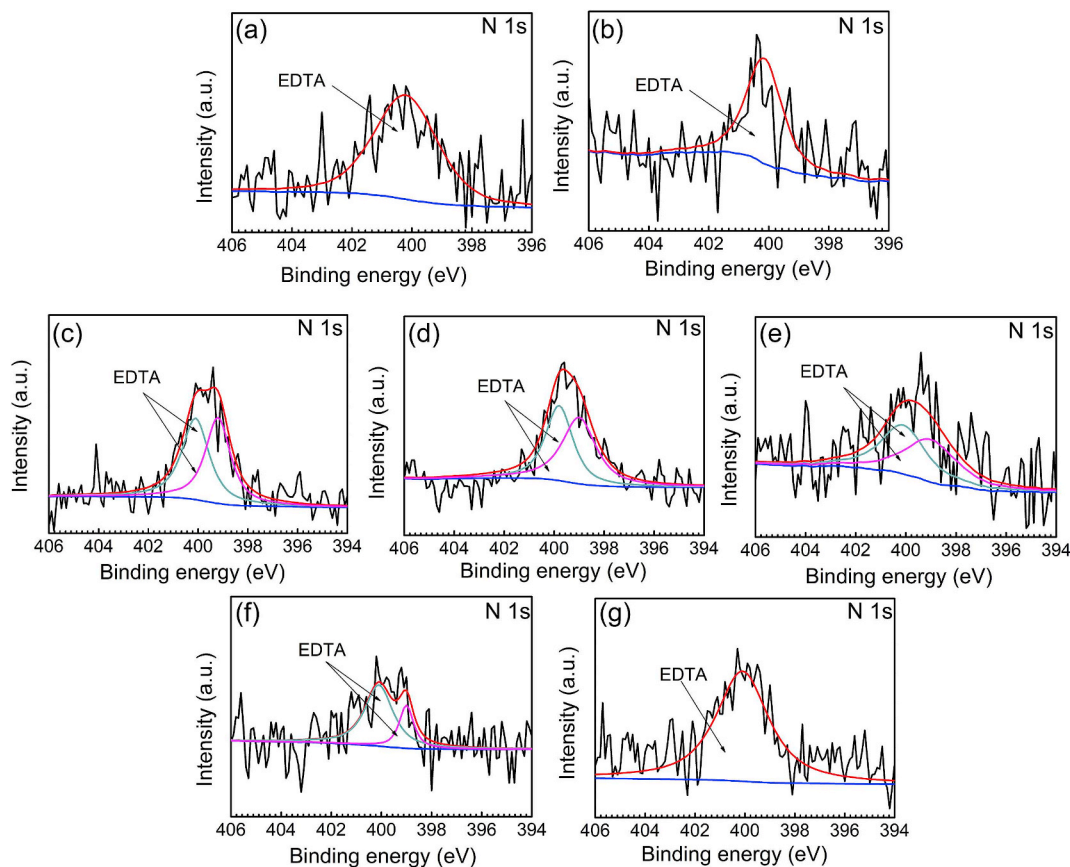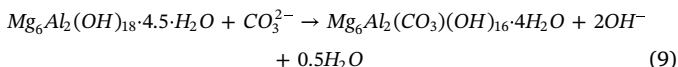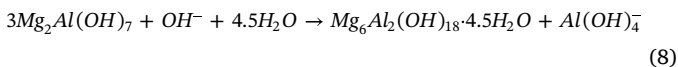
Fig. 15. XPS spectrums of the peak of N 1s of the MAO-LDH coatings at various soaking time: 1 min (a), 10 min (b), 1 h (c), 6 h (d), 12 h (e), 24 h (f), and 48 h (g).

$$3Mg_2Al(OH)_7 + OH^- + 4.5H_2O \rightarrow Mg_6Al_2(OH)_{18} \cdot 4.5H_2O + Al(OH)_4^-$$
$$(8)$$

$$Mg_6Al_2(OH)_{18} \cdot 4.5 \cdot H_2O + CO_3^{2-} \rightarrow Mg_6Al_2(CO_3)(OH)_{16} \cdot 4H_2O + 2OH^-$$
$$+ 0.5H_2O \qquad (9)$$

After soaking for 1 h (Fig. 14d–g), a large amount of Al^{3+} ions is adsorbed on MAO surface and more Mg^{2+} ions on the $Mg(OH)_2$ layer are replaced by Al^{3+}, resulting in the formation of the LDH coating on the MAO coating on AZ31 substrate.

4.1.4. Influence of the EDTA

EDTA has a strong complexing ability with metal ions, which may promote the deposition of free Al^{3+} ions in the solution onto MAO surface [45]. To further explore the role of EDTA, curve fitting of high-resolution N 1s peaks of MAO-coated Mg alloys immersed for different time is showed in Fig. 15. The existance of N in entire soaking process implies that EDTA constantly complexes free metal ions. This result is different from our previous research of the formation of $Mg(OH)_2$. EDTA only complexes with Mg^{2+} ions in the early stage of immersion, which may be that the growth of $Mg(OH)_2$ results in the decrease of free Mg^{2+} ions at substrate/solution interface. However, the solution B contains a large amount of free Al^{3+} ions in this experiment, which results in continuous complexation of EDTA. Moreover, Y^{4-} is dominant in the form of EDTA in solution when the pH is more than 10 [30,46,47]. And its complexation with Mg^{2+} ions and Al^{3+} ions are as follows:

$$Mg^{2+} + Y^{4-} \rightarrow MgY^{2-} \qquad (10)$$

$$Al^{3+} + Y^{4-} \rightarrow AlY^- \qquad (11)$$
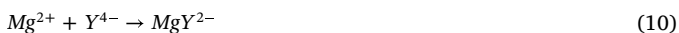
Therefore, EDTA complexes with the free Mg^{2+} ions on the MAO surface in the early stage of immersion, and continuously complexes

with the free Al^{3+} ions in the solution during the whole soaking process, which accelerates the deposition of Al^{3+} ions on MAO surface. In other words, the presence of EDTA promotes the growth of the LDH coating.

It is concluded that the dissolution of anodic α-Mg phase near AlMn particles, adsorption of Al^{3+} ions and the formation of $Mg(OH)_2$ and Al $(OH)_3$ occur. Subsequently, some of Mg^{2+} ions in the $Mg(OH)_2$ precipitates are replaced by Al^{3+} ions, and CO_3^{2-} ions are adsorbed, resulting in the formation of the LDH coating. The formation process of the LDH layer can be divided into four stages (Fig. 16):

(a) The dissolution of α-Mg near the AlMn phase (Eqs. (1)–(3)), the complexation of EDTA with Mg^{2+} and Al^{3+} ions (Eqs. (10 and (11)) and the hydroxide formation of $Mg(OH)_2$ and $Al(OH)_3$ (Eqs. (3) and (5));
(b) The transformation of MgO in the MAO coating into $Mg(OH)_2$ (Eq. (4));
(c) The partial Mg^{2+} ions in the $Mg(OH)_2$ by the substitution of Al^{3+} ions, and the adsorption of CO_3^{2-} ions;
(d) The massive deposition of Al^{3+} ions and the growth of the LDH coating (Eqs. (6)–(9)).

5. Conclusions

A preparation method of Mg–Al LDH coating suitable for MAO coating surface via *in-situ* growth at low temperature (60 °C) with higher pH (13.76) has been investigation. The major conclusions are drawn as following:

1) A low temperature and a high pH value successfully balance between the dissolution of the MAO coating and the growth of the LDH coating on Mg alloy AZ31. The dissolution of α-Mg and the growth
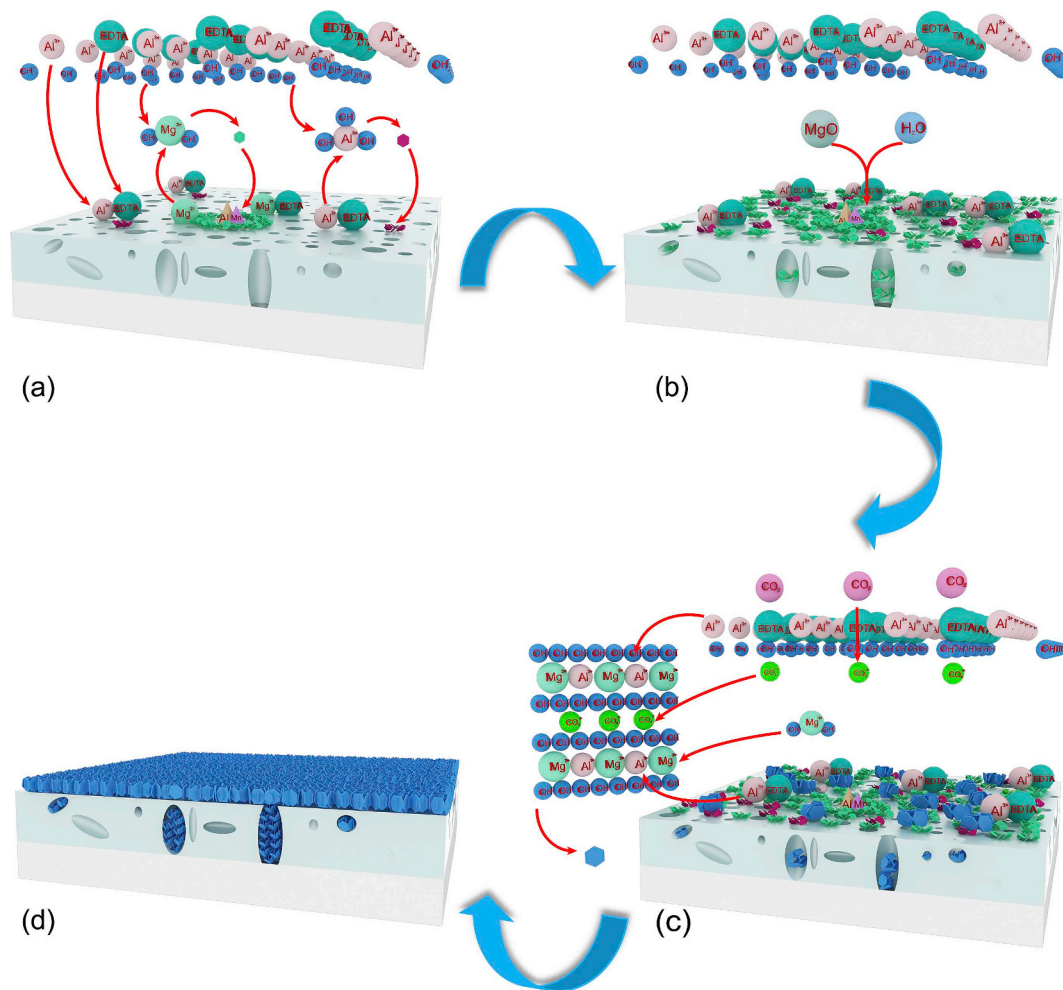
Fig. 16. Schematic diagram of growth mechanism of the MAO-LDH coating.

of $Mg(OH)_2$ initiates at intermetallic compounds Al–Mn particles. EDTA accelerates the deposition of Al^{3+} and thus the growth of LDH coating.

2) The corrosion current density of the MAO-LDH coating decreases four orders of magnitude than that of the substrate, and two orders of magnitude than that of the MAO coating. Moreover, the MAO-LDH coating exhibits a huge passivation region (approximately 0.6 V SCE^{-1}) in the anodic polarization branch, designating strong seal-healing ability due to the diffusion and ion-exchangeable behavior of the LDH coating. During the long immersion process, the MAO-LDH coating remains intact without cracking, and the nanosheet-like structure of the LDH is maintained. And nanosheet structured LDH was more conducive to the deposition of Ca–P products. Namely, MAO-LDH coating shows excellent corrosion resistance.

3) MTT assay and live/dead staining revealed that the MAO-LDH coating had acceptable biocompatibility for MC3T3-E1 osteoblasts. Thence, the MAO-LDH coating has a potential application value in orthopedic bone implant materials.

CRediT authorship contribution statement

Chang-Yang Li: Methodology, Investigation, Data curation, Writing - original draft. **Ling Gao:** Resources. **Xiao-Li Fan:** Software, Writing - review & editing. **Rong-Chang Zeng:** Conceptualization, Funding acquisition, Writing - review & editing. **Dong-Chu Chen:** Supervision. **Ke-Qian Zhi:** Supervision.

Declaration of competing interest

None.

References

[1] Y. Liu, Y.F. Zheng, X.H. Chen, J.A. Yang, H.B. Pan, D.F. Chen, L.N. Wang, J.L. Zhang, D.H. Zhu, S.L. Wu, K.W.K. Yeung, R.C. Zeng, Y. Han, S.K. Guan, Fundamental theory of biodegradable metals—definition, criteria, and design, Adv. Funct. Mater. 29 (2019) 1–21.

[2] M.C. Zhao, Y.C. Zhao, D.F. Yin, S. Wang, Y.M. Shangguan, C. Liu, L.L. Tan, C.J. Shuai, K. Yang, A. Atrens, Biodegradation behavior of coated as-extruded Mg–Sr alloy in simulated body fluid, Acta Metall. Sin. (Engl. Lett.) 32 (2019) 1195–1206.

[3] C. Song, Y.X. Yang, Y.F. Zhou, L.G. Wang, S.J. Zhu, J.F. Wang, R.C. Zeng, Y.F. Zheng, S.K. Guan, Electrochemical polymerization of dopamine with/without subsequent PLLA coating on Mg-Zn-Y-Nd alloy, Mater. Lett. 252 (2019) 202–206.

[4] L. Mao, L. Shen, J. Niu, J. Zhang, W. Ding, Y. Wu, R. Fan, G. Yuan, Nanophasic biodegradation enhances the durability and biocompatibility of magnesium alloys for the next-generation vascular stents, Nanoscale 5 (2013) 9517–9522.

[5] P. Liu, J.M. Wang, X.T. Yu, X.B. Chen, S.Q. Li, D.C. Chen, S.K. Guan, R.C. Zeng, L.Y. Cui, Corrosion resistance of bioinspired DNA-induced Ca-P coating on biodegradable magnesium alloy, J. Magn. Alloys 7 (2019) 144–154.

[6] J.A. Li, L. Chen, X.Q. Zhang, S.K. Guan, Enhancing biocompatibility and corrosion resistance of biodegradable Mg-Zn-Y-Nd alloy by preparing PDA/HA coating for potential application of cardiovascular biomaterials, Mater. Sci. Eng. C 109 (2020).

[7] Y.B. Zhao, X.B. Chen, S.Q. Li, R.C. Zeng, F. Zhang, Z.L. Wang, S.K. Guan, Corrosion resistance and drug release profile of gentamicin-loaded polyelectrolyte multilayers on magnesium alloys: effects of heat treatment, J. Colloid Interface Sci. 547 (2019) 309–317.

[8] L.Y. Li, L.Y. Cui, B. Liu, R.C. Zeng, X.B. Chen, S.Q. Li, Z.L. Wang, E.H. Han, Corrosion resistance of glucose-induced hydrothermal calcium phosphate coating on pure magnesium, Appl. Surf. Sci. 465 (2019) 1066–1077.

[9] X. Yan, M.C. Zhao, Y. Yang, L. Tan, Y.C. Zhao, D.F. Yin, K. Yang, A. Atrens, Improvement of biodegradable and antibacterial properties by solution treatment and micro-arc oxidation (MAO) of a magnesium alloy with a trace of copper, Corros. Sci. 156 (2019) 125–138.

[10] Y. Li, H. Li, Q. Xiong, X. Wu, J. Zhou, J. Wu, X. Wu, W. Qin, Multipurpose surface functionalization on AZ31 magnesium alloys by atomic layer deposition: tailoring the corrosion resistance and electrical performance, Nanoscale 9 (2017) 8591–8599.

[11] L.Y. Cui, R.C. Zeng, S.K. Guan, W.C. Qi, F. Zhang, S.Q. Li, E.H. Han, Degradation mechanism of micro-arc oxidation coatings on biodegradable Mg-Ca alloys: the influence of porosity, J. Alloys Compd. 695 (2017) 2464–2476.

[12] Q.S. Yao, Z.C. Li, Z.M. Qiu, F. Zhang, X.B. Chen, D.C. Chen, S.K. Guan, R.C. Zeng, Corrosion resistance of $Mg(OH)_2/Mg$-Al-layered double hydroxide coatings on magnesium alloy AZ31: influence of hydrolysis degree of silane, Rare Met. 38 (2019) 629–641.

[13] Q.S. Yao, F. Zhang, L. Song, R.C. Zeng, L.Y. Cui, S.Q. Li, Z.L. Wang, E.H. Han, Corrosion resistance of a ceria/polymethyltrimethoxysilane modified Mg-Al-layered double hydroxide on AZ31 magnesium alloy, J. Alloys Compd. 764 (2018) 913–928.

[14] G. Zhang, L. Wu, A. Tang, B. Weng, A. Atrens, S.D. Ma, L. Liu, F.S. Pan, Sealing of anodized magnesium alloy AZ31 with MgAl layered double hydroxides layers, RSC Adv. 8 (2018) 2248–2259.

[15] J. Lin, C. Hsia, J. Uan, Characterization of Mg, Al-hydrotalcite conversion film on Mg alloy and Cl^- and CO_3^{2-} anion-exchangeability of the film in a corrosive environment, Scripta Mater. 56 (2007) 927–930.

[16] G. Zhang, L. Wu, A. Tang, S. Zhang, B. Yuan, Z.C. Zheng, F.S. Pan, A novel approach to fabricate protective layered double hydroxide films on the surface of anodized Mg-Al alloy, Adv. Mater. Interfaces 4 (2017) 1700163.

[17] R.C. Zeng, Z.G. Liu, F. Zhang, S.Q. Li, H.Z. Cui, E.H. Han, Corrosion of molybdate intercalated hydrotalcite coating on AZ31 Mg alloy, J. Mater. Chem. 2 (2014) 13049–13057.

[18] F. Peng, D.H. Wang, Y.X. Tian, H.L. Cao, Y.Q. Qiao, X.Y. Liu, Sealing the pores of PEO coating with Mg-Al layered double hydroxide: enhanced corrosion resistance, cytocompatibility and drug delivery ability, Sci. Rep. 7 (2017) 8167–8178.

[19] F. Peng, H. Li, D.H. Wang, P. Tian, Y.X. Tian, G.Y. Yuan, D. Xu, X.Y. Liu, Enhanced corrosion resistance and biocompatibility of magnesium alloy by Mg-Al-Layered double hydroxide, ACS Appl. Mater. Interfaces 8 (2016) 35033–35044.

[20] Y.X. Chen, R. Zhu, Q.F. Ke, Y.S. Gao, C.Q. Zhang, Y.P. Guo, MgAl layered double hydroxide/chitosan porous scaffolds loaded with PFTalpha to promote bone regeneration, Nanoscale 9 (2017) 6765–6776.

[21] F. Zhang, Z.G. Liu, R.C. Zeng, S.Q. Li, H.Z. Cui, L. Song, E.H. Han, Corrosion resistance of Mg-Al-LDH coating on magnesium alloy AZ31, Surf. Coating. Technol. 258 (2014) 1152–1158.

[22] T. Ishizaki, S. Chiba, K. Watanabe, H. Suzuki, Corrosion resistance of Mg−Al layered double hydroxide container-containing magnesium hydroxide films formed directly on magnesium alloy by chemical-free steam coating, J. Mater. Chem. 1 (2013) 8968–8977.

[23] S.F. Li, Y.M. Shen, D.B. Liu, L.H. Fan, X.C. Zheng, J. Yang, One-step fabrication of oriented Mg/Al-layered double hydroxide film on magnesium substrate with urea hydrolysis and its corrosion resistance, Compos. Interfac. 19 (2013) 489–498.

[24] J. Chen, Y.W. Song, D.Y. Shan, E.H. Han, In situ growth of Mg−Al hydrotalcite conversion film on AZ31 magnesium alloy, Corros. Sci. 53 (2011) 3281–3288.

[25] J. Chen, Y.W. Song, D.Y. Shan, E.H. Han, Study of the in situ growth mechanism of Mg−Al hydrotalcite conversion film on AZ31 magnesium alloy, Corros. Sci. 63 (2012) 148–158.

[26] J. Chen, Y.W. Song, D.Y. Shan, E.H. Han, In situ growth process of Mg−Al hydrotalcite conversion film on AZ31 Mg alloy, J. Mater. Sci. Technol. 31 (2015) 384–390.

[27] J. Chen, W. Lin, S. Liang, L. Zou, C. Wang, B. Wang, M. Yan, X. Cui, Effect of alloy cations on corrosion resistance of LDH/MAO coating on magnesium alloy, Appl. Surf. Sci. 463 (2019) 535–544.

[28] D. Jiang, X.C. Xia, J. Hou, G.Y. Cai, X.X. Zhang, Z.H. Dong, A novel coating system with self-reparable slippery surface and active corrosion inhibition for reliable protection of Mg alloy, Chem. Eng. J. 373 (2019) 285–297.

[29] A.A. Eliseev, A.V. Lukashin, A.A. Vertegel, V.P. Tarasov, A study of crystallization of Mg–Al double hydroxides, Dokl. Chem. 387 (2002) 339–343.

[30] C.Y. Li, X.L. Fan, R.C. Zeng, L.Y. Cui, S.Q. Li, F. Zhang, Q.K. He, M.B. Kannan, H.W. Jiang, D.C. Chen, S.K. Guan, Corrosion resistance of in-situ growth of nano-sized $Mg(OH)_2$ on micro-arc oxidized magnesium alloy AZ31-Influence of EDTA, J. Mater. Sci. Technol. 35 (2019) 1088–1098.

[31] X.J. Ji, L. Gao, J.C. Liu, J. Wang, Q. Cheng, J.P. Li, S.Q. Li, K.Q. Zhi, R.C. Zeng, Z.L. Wang, Corrosion resistance and antibacterial properties of hydroxyapatite coating induced by gentamicin-loaded polymeric multilayers on magnesium alloys, Colloids Surf., B 179 (2019) 429–436.

[32] C.Y. Li, X.L. Feng, X.L. Fan, X.T. Yu, Z.Z. Yin, M.B. Kannan, X.B. Chen, S.K. Guan, J. Zhang, R.C. Zeng, Corrosion and wear resistance of micro-arc oxidation composite coatings on magnesium alloy AZ31-The influence of inclusions of carbon spheres, Adv. Eng. Mater. 21 (2019) 1–16.

[33] R.C. Zeng, Z.G. Liu, F. Zhang, S.Q. Li, Q.K. He, H.Z. Cui, E.H. Han, Corrosion resistance of in-situ Mg–Al hydrotalcite conversion film on AZ31 magnesium alloy by one-step formation, Trans. Nonferrous Metals Soc. China 25 (2015) 1917–1925.

[34] R. Zeng, K.U. Kainer, C. Blawert, W. Dietzel, Corrosion of an extruded magnesium alloy ZK60 component—the role of microstructural features, J. Alloys Compd. 509 (2011) 4462–4469.

[35] C.S. Xiong, W.H. Li, X. Gao, W. Wang, H.W. Tian, P. Han, L.Y. Song, L.H. Jiang, Preparation of phytic acid conversion coating and corrosion protection performances for steel in chlorinated simulated concrete pore solution, Corros. Sci. 139 (2018) 275–288.

[36] Y.L. Wang, S.H. Zhang, Z.X. Lu, L.S. Wang, W.H. Li, Preparation and performances of electrically conductive Nb-doped TiO2 coatings for 316 stainless steel bipolar plates of proton-exchange membrane fuel cells, Corros. Sci. 142 (2018) 249–257.

[37] K. Yin, H.W. Liu, Y.F. Cheng, Microbiologically influenced corrosion of X52 pipeline steel in thin layers of solution containing sulfate-reducing bacteria trapped under disbonded coating, Corros. Sci. 145 (2018) 271–282.

[38] Y.N. Singhbabu, B. Sivakumar, J.K. Singh, H. Bapari, A.K. Pramanick, R.K. Sahu, Efficient anti-corrosive coating of cold-rolled steel in a seawater environment using an oil-based graphene oxide ink, Nanoscale 7 (2015) 8035–8047.

[39] X. Zhou, H.Y. Yang, F.H. Wang, Investigation on the inhibition behavior of a pentaerythritol glycoside for carbon steel in 3.5% NaCl saturated $Ca(OH)_2$ solution, Corros. Sci. 54 (2012) 193–200.

[40] Y.H. Cao, S.G. Dong, D.J. Zheng, J.J. Wang, X.J. Zhang, R.G. Du, G.L. Song, C.J. Lin, Multifunctional inhibition based on layered double hydroxides to comprehensively control corrosion of carbon steel in concrete, Corros. Sci. 126 (2017) 166–179.

[41] L. Chen, J.G. Li, S. Wang, S.J. Zhu, C. Zhu, B.Y. Zheng, G. Yang, S.K. Guan, Surface modification of the biodegradable cardiovascular stent material Mg–Zn–Y–Nd alloy via conjugating REDV peptide for better endothelialization, J. Mater. Res. 33 (2018) 4123–4133.

[42] J.L. Wang, F. Witte, T.F. Xi, Y.F. Zheng, K. Yang, Y.S. Yang, D.W. Zhao, J. Meng, Y.D. Li, W.R. Li, K.M. Chan, L. Qin, Recommendation for modifying current cytotoxicity testing standards for biodegradable magnesium-based materials, Acta Biomater. 21 (2015) 237–249.

[43] Z. Cui, Y. Zhang, Y. Cheng, D. Gong, W. Wang, Microstructure, mechanical, corrosion properties and cytotoxicity of betacalcium polyphosphate reinforced ZK61 magnesium alloy composite by spark plasma sintering, Mater. Sci. Eng. C Mater. Biol. Appl. 99 (2019) 1035–1047.

[44] J. Kubasek, D. Vojtech, E. Jablonska, I. Pospisilova, J. Lipov, T. Ruml, Structure, mechanical characteristics and in vitro degradation, cytotoxicity, genotoxicity and mutagenicity of novel biodegradable Zn-Mg alloys, Mater. Sci. Eng. C Mater. Biol. Appl. 58 (2016) 24–35.

[45] X.L. Fan, Y.F. Huo, C.Y. Li, M.B. Kannan, X.B. Chen, S.K. Guan, R.C. Zeng, Q.L. Ma, Corrosion resistance of nanostructured magnesium hydroxide coating on magnesium alloy AZ31: influence of EDTA, Rare Met. 38 (2019) 520–531.

[46] J.B. Liu, K.W. Li, H. Wang, M.K. Zhu, H.Y. Xu, H. Yan, Self-assembly of hydroxyapatite nanostructures by microwave irradiation, Nanotechnology 16 (2005) 82–87.

[47] S.P. Wang, R.H. Liu, J. Yao, Y. Wang, H.R. Li, R.N. Dao, J. Guan, G.P. Tang, Fabrication of mesoporous magnesium substituted β-tricalcium phosphate nanospheres by self-transformation and assembly involving EDTA ions, Microporous Mesoporous Mater. 179 (2013) 172–181.